JOURNAL OF THERMOPHYSICS AND HEAT TRANSFER
Vol. 14, No. 4, October–December 2000

Multidimensional Monte Carlo Simulation of Short-Pulse Laser Transport in Scattering Media

Zhixiong Guo,* Sunil Kumar,† and Kuo-Ching San‡
Polytechnic University, Brooklyn, New York 11201

The Monte Carlo technique is used to simulate the two-dimensional transient radiative heat transfer in scattering and absorbing media. The transient behavior of transmissivity and reflectivity, subject to short-pulse laser radiation incident on highly scattering media, is investigated. The influences of medium dimensions, anisotropic scattering characteristics, incident pulse width and spatial and temporal Gaussian distributions, and the effect of Fresnel reflection resulting from refractive index changes at the boundaries are discussed. It is found that the temporal distribution shape and spread of the predicted transmissivity and reflectivity are significantly influenced by the incident pulse width and the dimensions of the media. Forward scattering increases the magnitude of maximum transmissivity and reduces the transmitted pulse width. Neglecting the boundary reflection results in overestimated transmissivity and reflectivity and shortens the transmitted pulse width.

Nomenclature

A_1	=	linear anisotropic scattering coefficient
c	=	speed of light through medium, mm/ps
c_0	=	speed of light in vacuum, = 0.3 mm/ps
D	=	path length, mm
$H(t)$	=	Heaviside function
I_c	=	incident laser intensity, W/m^2
I_1	=	maximum value of Gaussian input pulse intensity
I_2	=	maximum value of step input pulse intensity
L	=	thickness, mm
n_s	=	refractive index
R	=	random number between 0 and 1
r	=	radial coordinate
r_i	=	radius of incident laser beam, mm
$\hat{\boldsymbol{s}}$	=	unit direction vector
t	=	time, ps
t_1	=	start time of input pulse, ps
t_2	=	end time of input pulse, ps
t_p	=	pulse width of incident laser, ps
W	=	width, mm
x, y, z	=	Cartesian coordinates
θ	=	polar angle
θ'	=	polar angle measured from an axis pointing in the incoming light direction
θ_i	=	incident angle
θ_r	=	refractive angle
ρ	=	reflectance
σ_e	=	extinction coefficient, mm^{-1}
Φ	=	scattering phase function
ψ	=	circumferential angle
ψ'	=	circumferential angle measured in a plane normal to the incoming light direction
ω	=	scattering albedo

Received 7 September 1999; revision received 13 March 2000; accepted for publication 7 April 2000.

*Research Associate, Department of Mechanical Engineering, 6 Metrotech Center; zguo@poly.edu.

†Department Head, Department of Mechanical, Aerospace, and Manufacturing Engineering, 6 Metrotech Center; skumar@poly.edu. Senior Member AIAA.

‡Graduate Student, Department of Mechanical Engineering, 6 Metrotech Center.

Introduction

IN the past decade, many researchers have focused on evaluating the propagation and scattering characteristics of short-pulse light transport through highly scattering media. Many applications have burgeoned due to the advent of the short-pulse laser. Examples are optical tomography of tissue, remote sensing of oceans and atmospheres, laser material processing of microstructures, and the possibilities of using short-pulse x rays for noninvasive diagnostics. A review by Kumar and Mitra[1] summarized the microscale aspects of thermal radiation transport and short-pulse laser applications.

Significant progress has been made in the development of solution methods for multidimensional radiative heat transfer in participating media in recent years. However, the analysis of radiative heat transfer in most engineering problems traditionally neglects the effect of speed-of-light propagation, even if the boundary conditions and/or the sources that are responsible for the radiative intensity vary with time. With laser pulse widths as short as picoseconds to femtoseconds,[2] neglecting the time dependence of radiative transport may induce significant errors in the prediction of transient radiation heat transfer.

Very few studies have addressed transient radiative transport. Kumar and Mitra[3] and Kumar et al.[4] are among the first to consider the entire transient radiative equation by using a variety of models for short-pulse applications. Mitra et al.[5] solve the two-dimensional wavelike transient radiative transfer equation using the P_1 approximation for a boundary-driven problem. Mitra and Kumar[6] compare several numerical models for the prediction of light pulse transport through one-dimensional scattering–absorbing media. Previously, the transient radiative transfer equation, with a source of constant strength at the boundaries, had been solved using Laplace transforms and adding-doubling methods.[7,8] Other formulations considering the entire hyperbolic radiative equation for laser pulses have not been covered in the literature, except for a brief discussion by Ishimaru.[9] Most studies consider the parabolic transient P_1 diffusion approximation, obtained by dropping certain time derivatives to parabolize the transfer equation.[10] Some of these studies have also experimentally investigated short-pulse laser transport through tissues, where the scattering albedo is very large, and have indicated that the P_1 diffusion approximation is adequate for optically thick tissue samples. However, these parabolic models have not matched experimental results in other studies.[11]

Although one-dimensional transient radiative heat transfer has been discussed broadly, the study of multidimensional transient radiative transfer is sparse. Moreover, a more realistic simulation of short-pulse laser transport is required, which would include the input of a realistic laser beam, the boundary reflection due to the

change of refractive index, and the characteristics of anisotropically scattering media. Many approaches were used in the references mentioned, but few can easily and efficiently treat all of these realistic complications. One viable approach is the Monte Carlo method, even though it is subject to computational expense and statistical error.

Monte Carlo methods have been used extensively in steady-state simulations of radiative heat transfer.[12–18] General reviews by Siegel and Howell[12] and Modest[13] provided the details for implementation of the method. Recently, researchers have started using the Monte Carlo method to address transient laser-tissue interactions. Wilson and Adam[19] developed a Monte Carlo model to study the propagation of light in tissue, in which boundary reflections and time derivatives were ignored and scattering was assumed to be isotropic. Anisotropic scattering was considered in the Monte Carlo methods developed by Deply et al.[20] and Jacques.[21] Flock et al.[22] and Madsen et al.[23] have tested Monte Carlo results by comparison with diffusion theory and experimental measurement. Hasegawa et al.[24] employed the Monte Carlo method to trace the paths of rays incident upon slabs containing either two types of scattering particles or one type of particle with pigment. Takahashi et al.[25] incorporated a boundary reflection and found that it broadened the transmitted pulse width. The Monte Carlo method was also used to investigate the feasibility of determining optical properties of turbid media from time-resolved light scattering measurement.[26] In these studies,[19–26] however, an instantaneous, isotropic point source was used to simulate the incident laser beam; Gaussian temporal and spatial profiles were not considered; boundary reflection was not generally taken into account; and the system was generally restricted to a one-dimensional slab. A literature survey reveals that no publication is available depicting work involving multidimensional simulation of transient laser transport with realistic physical conditions.

In the present treatise, a Monte Carlo approach is developed to simulate two-dimensional transient radiative transport of a short-pulse laser beam incident upon highly scattering media. Realistic physical models are incorporated, such as temporal and spatial Gaussian distributions of the laser beam, Fresnel reflection at the media/air boundaries, and anisotropic scattering characteristics. The temporal transmitted and reflected fluxes are obtained over a broad range of various parameters, such as thickness and width of the media, and the temporal width and spatial radius of the incident laser. The influences of the geometric dimensions, the features of the incident beam, and the location of the detecting point are discussed. The effects of boundary reflection and anisotropic scattering characteristics of the media are examined.

Analytical Model

The medium geometry, coordinates, and input laser pulse are depicted in Fig. 1. The pulsed laser is normally incident upon the participating medium from the origin of the Cartesian coordinates. The incident laser intensity has temporal and spatial Gaussian profiles and can be expressed as

$$I_c(r, z = 0, t) = I_1 \exp\left[-4\ln 2 \times \left(\frac{t - t_p/2}{t_p}\right)^2\right] \times \exp(-r^2/v^2) \tag{1}$$

where t_p, termed pulse width, is full width at half maximum (FWHM) and $v^2/2$ is the spatial variance.

A step function is usually adopted to simulate the incident pulse for many transient radiative transfer analysis methods. A temporal square-wave pulse can be expressed by the Heaviside step function as

$$I_c(r, z = 0, t) = I_2[H(t) - H(t - t_p)] \times \exp(-r^2/v^2) \tag{2}$$

For the sake of comparison, we set the FWHM of the input Gaussian pulse to coincide with that of the input step pulse as shown in Fig. 1. Therefore, the step input pulse starts at $t_1 = 0$ and ends at $t_2 = t_p$, whereas the input Gaussian pulse is started at $t_1 = -2t_p$ and ended at $t_2 = 3t_p$.

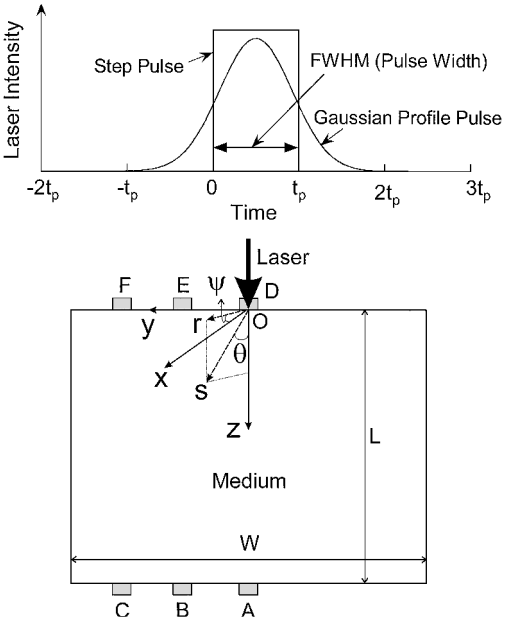

Fig. 1 Sketches of medium geometry, coordinates, and input laser pulse profiles.

The geometric dimensions are L in thickness in the z direction, W in width in the y direction, and infinite in the x direction. The extinction coefficient σ_e of the participating medium is assumed to be uniform and constant at 1.0 mm^{-1}. The scattering albedo ω is as high as 0.997. A high value of scattering albedo is selected because it corresponds to the more difficult cases to simulate. Lower values of albedo, indicative of smaller magnitude of scattering and high absorption, are relatively easier to simulate. Also, high albedo is characteristic of an important application: time-resolved laser tomography of tissues.[24] The anisotropic scattering of living tissue could be conveniently specified by the Henyey–Greenstein phase function as was done by Jacques.[21] Although the Monte Carlo method is general and any type of anisotropic scattering can be utilized, for simplicity, we assume linear anisotropic scattering in the present investigation as follows:

$$\Phi(\hat{s} \cdot \hat{s}') = 1 + A_1 \hat{s} \cdot \hat{s}' = 1 + A_1 \cos\theta' \tag{3}$$

The linear anisotropic phase function reduces the number of independent parameters needed for characterizing the scattering to only one: the variable A_1. For positive values of A_1, it is forward scattering. In contrast, it is backward scattering for negative values of A_1.

Fresnel reflection is taken into account at the input and output interfaces that are exposed to air. Snell's law is obeyed:

$$n_s \sin\theta_i = \sin\theta_r \tag{4}$$

in which the incident angle is θ_i and refraction angle is θ_r. Because the refractive index of the medium, $n_s > 1$, total reflection occurs at the boundaries when $\theta_i \geq \sin^{-1}(1/n_s)$. When $\theta_i < \sin^{-1}(1/n_s)$, the reflectance between the random walk medium and air is given by the Fresnel equation as

$$\rho = \frac{1}{2}\left[\frac{\tan^2(\theta_i - \theta_r)}{\tan^2(\theta_i + \theta_r)} + \frac{\sin^2(\theta_i - \theta_r)}{\sin^2(\theta_i + \theta_r)}\right] \tag{5}$$

Monte Carlo Method

The Monte Carlo method is a rather flexible technique. It has been applied to a wide variety of problems. It can handle nearly any physical condition as long as it can be represented by the appropriate probability distributions, which in turn are simulated by repetitions of random numbers generated by the computer. In the

Monte Carlo approach, radiative transfer is simulated using the calculated movements of a statistically large number of radiative energy bundles. As each bundle proceeds from its initial location and initial emission time through the participating medium, it experiences scattering, reflection, and absorption. On completion of the simulation, predictions of heat transfer are determined based on the averaged behavior of the set of individual energy bundles. The difficulties inherent in the solution of the time-dependent, integro-differential radiative transfer equation and the complexity in dealing with the Fresnel reflection and anisotropic scattering can be avoided.

Except the transient behavior, the traditional Monte Carlo algorithm has been described in common textbooks[12,13] in detail. In the present study, the emission points are determined from the laser beam source. The position (r, ψ) of the incidence of the laser photon bundles on the $z = 0$ interface is derived as

$$R = \frac{\int_0^r \int_0^{2\pi} I_c(r', t) r' \, d\theta \, dr'}{\int_0^{r_i} \int_0^{2\pi} I_c(r', t) r' \, d\theta \, dr'} = \frac{1 - \exp(-r^2/v^2)}{1 - \exp\left(-r_i^2/v^2\right)} \tag{6}$$

$$R = \frac{\int_0^{\psi} I_c(r, t) \, d\psi'}{\int_0^{2\pi} I_c(r, t) \, d\psi'} = \frac{\psi}{2\pi} \tag{7}$$

in which R is a random number. In Cartesian coordinates, the location of the emission point is

$$x = r \cos\psi, \qquad y = r \sin\psi, \qquad z = 0 \tag{8}$$

The initial time of the incident energy bundle in one pulse is determined by

$$R = \frac{\int_{t_1}^{t} I_c(r, t') \, dt'}{\int_{t_1}^{t_2} I_c(r, t') \, dt'} \tag{9}$$

For a temporally square pulse, the initial time is easily calculated by

$$t = Rt_p \tag{10}$$

For a temporally Gaussian pulse, the initial time is determined by the inverse calculation of the error function. Note that the initial time may be less than $t = 0$ for a Gaussian pulse because the pulse is started at $t_1 = -2t_p$.

The present method determines the photon initial emission time by using the Monte Carlo technique. The traits of such a treatment are the following: the time-resolution can be infinitesimal, all photon bundles have the same amount of energy, and the total number of emission bundles is fixed. Equation (9) is valid for any type of temporal-pulse variation. To the authors' knowledge, no treatment similar to Eq. (9) has been published in the open literature.

The initial direction of the incident laser bundle is

$$\theta = 0 \tag{11}$$

i.e., the laser is assumed to be incident perpendicular on the surface.

The distance that any one bundle may travel before absorption or scattering is

$$D = (1/\sigma_e) \ln(1/R) \tag{12}$$

The deposit fraction by absorption is $1 - \omega$. For temporal analysis, the total optical path length of each ray inside the medium is converted to time of flight by using the speed of light in the medium:

$$t = D/c = Dn_s/c_0 \tag{13}$$

The direction of light propagation after scattering is determined by the scattering phase function. For isotropic scattering,

$$\psi = 2\pi R, \qquad \theta = \cos^{-1}(1 - 2R) \tag{14}$$

For linear anisotropic scattering, the new angles after a scattering event are

$$\psi' = 2\pi R \tag{15}$$

$$\theta' = \cos^{-1}\left[\frac{\sqrt{1 - 2A_1(1 - 2R) + A_1^2} - 1}{A_1}\right] \tag{16}$$

where the polar angle θ' is measured from an axis pointing in the incoming direction of the radiation and the circumferential angle ψ' is measured in a plane normal to the incoming direction. Programming for anisotropic scattering needs a transformation of coordinate systems, which results in a much longer computation time than that for isotropic scattering. Because anisotropic scattering can be scaled into equivalent isotropic scattering with good results,[27] most of the present calculations are performed for isotropically scattering media if not specifically noted otherwise. However, anisotropic scattering is included in the present algorithm and the effect of anisotropic scattering characteristics is discussed.

Each photon bundle is traced until it escapes from the boundaries of the medium or the total flight time is over 600 ps. For a highly scattering medium ($\omega = 0.997$) with Fresnel reflective boundaries, a few rays may scatter or reflect thousands of times inside the medium before being fully absorbed or transmitted. As a result, the computational time is substantially increased. To reduce the CPU time, a ray scattering and/or reflecting over 1000 times inside the medium is not traced further. Because the ray energy has been reduced to less than 5% of its initial energy after 1000 scattering events, neglecting such rays results in a total energy error of less than 1% and has no obvious effect on the results. Comparison with nonlimited scattering events was conducted, and the general difference was found to be less than 1%.

The total number of emission bundles varied from 10^6 to 10^8. Several trial calculations were repeated to test the sensitivity of the results to the number of emission bundles. Convergent results were found, and the outcome of these exercises was satisfactory. The increase in the number of emission bundles will reduce the fluctuation of the prediction, and consequently, will improve accuracy but will also result in considerably longer computational time. In general, 10^7 bundles were chosen in the present study. However, 10^8 bundles were used in a few cases, as specifically indicated. The numerical algorithm was also checked by comparing its one-dimensional results with previous Monte Carlo predictions[21–24] for impulse-incident irradiation without boundary reflection. The outcome was satisfactory, and the difference was very small.

Results and Discussion

The transmitted and reflected fluxes at all of the boundaries and the absorbed flux inside the medium can be obtained by the present Monte Carlo simulation. However, the transmitted and reflected fluxes at the interfaces of $z = L$ and 0, respectively, are of prime interest in the study of short-pulse laser transport through participating media. The transmissivity (at $z = L$) and reflectivity (at $z = 0$) used in the following sections are defined as the transmitted and reflected energy normalized by the total incident laser energy. The basic values of parameters are $L = 10$ mm, $W = 10$ mm, $t_p = 10$ ps, $r_i = 1.0$ mm, $n_s = 1.33$, $\sigma_e = 1.0$ mm^{-1}, and $\omega = 0.997$. The spatial variance v in the Gaussian profile beam is assumed to be equal to the radius of laser beam.

Effects of Temporal Gaussian Pulse and Detector Position

The temporal transmissivity and reflectivity distributions are varied according to the detector locations in the y direction. The locations of detectors for calculating transmissivity and reflectivity are listed in Table 1. The temporal transmissivity and reflectivity distributions are shown in Figs. 2 and 3, respectively. Comparisons are performed between one temporal Gaussian profile input pulse and one step-input pulse and among three different detector locations. The parameters used in the computation have their basic values as specified before. Figure 2 shows that there is a sudden

Table 1 Selected locations at the incident and transmitted interfaces: detector radius = 1 mm

Detector	Position, (x, y, z)	Property
Location A	$(0, 0, L)$	Transmissivity
Location B	$(0, 2, L)$	Transmissivity
Location C	$(0, 4, L)$	Transmissivity
Location D	$(0, 0, 0)$	Reflectivity
Location E	$(0, 2, 0)$	Reflectivity
Location F	$(0, 4, 0)$	Reflectivity

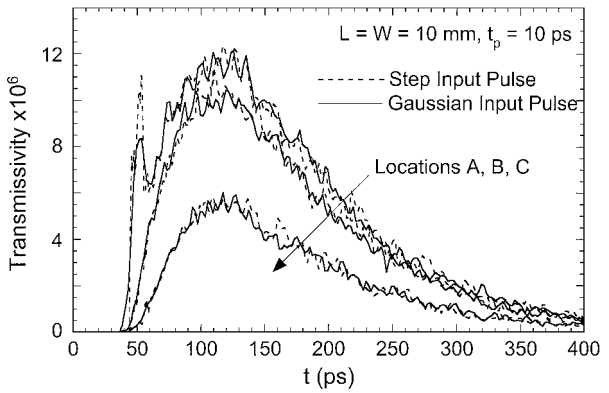

Fig. 2 Comparisons of temporal transmissivity at three different detector locations subject to different temporal variations of input pulse.

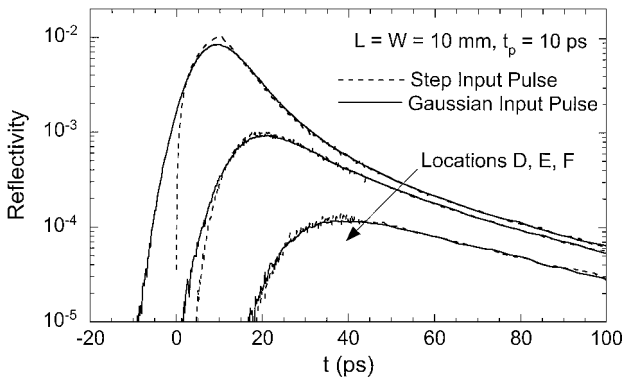

Fig. 3 Comparisons of temporal reflectivity at three different detector locations subject to different temporal variations of input pulse.

increase at an early time in the transmissivity profile at location A where its center coincides with the axis of the incident laser beam. Such a peak corresponds to the direct transmission of the laser beam through the medium without interaction. The peak value subject to the step-input pulse is larger than that of the Gaussian input pulse because the incident energy is more focused in a narrow time range. The initial response time subject to the step-input pulse equals the minimum time of light propagation in the medium, i.e., $t = L/c = L \times n_s/c_0 = 44.33$ ps. However, the detected initial response time, subject to the Gaussian input pulse, is earlier than that due to the step-input pulse because the Gaussian input pulse is started from $t = -2t_p$. The time variation of the input pulse affects the transmissivity profiles at an early time stage. After that, the influence of input pulse shape is not obvious. At locations B and C, there are no direct photons from the incident laser, so that the transmissivity profiles have no sudden increase at an early time. The transmitted pulses at locations B and C are produced because of multiple scattering of photons in the medium. The original arrival time of the photon has a slight influence on the transmissivity profiles at locations B and C. Thus, it is seen that the transmissivity profiles at locations B and C nearly coincide for Gaussian and step-input pulses. As expected, the magnitude of transmissivity decreases as the location of the detector moves from A to B to C. However, it is hard to see the influence of lateral location on the transmitted pulse width.

From Fig. 3, it is also found that the time variation of the input pulse affects the transient reflectivity only early in the time profile. The initial response time at location E is 0.0 ps for the step-input pulse, i.e., the start time of the input pulse. However, note that the start time for the Gaussian input pulse is $t = -2t_p$. Thus, the initial reflection response time is earlier than 0 ps. The maximum value of reflectivity subject to the step-input pulse is larger than that of the Gaussian input pulse. However, the reflected pulse width (FWHM) does not change, subject to various input pulses. As time elapses, the reflectivity at location D increases rapidly and reaches a maximum at a time approximately equal to the value of incident pulse width and then decreases rapidly until $t \cong 2t_p$. After that, it decreases gradually with a long decaying tail. As the detector moves from D to E to F, the initial response time delays and the value of the peak reflectivity decrease substantially. The reflected pulse width increases as the lateral location moves from the center of incidence.

From Figs. 2 and 3, it is also seen that the transmitted signal pulse width is much larger than that of the reflected pulse. This is because the reflectivity in the early time period is primarily due to the interaction of the incident pulse with material in the vicinity of the region of incidence, while the transmissivity in the long time period is the result of numerous multiple scattering events for light in the medium. Consequently, the magnitude of transmissivity is also much smaller than that of reflectivity for an optically thick medium.

The step-input pulse reduces the calculation effort and provides a benchmark for comparison with other methods. It also does not obviously influence the transmitted and reflected pulse widths and the distribution shapes (except for very early time). Therefore, we assume a square-wave step pulse as the incident laser pulse in the following sections.

Effect of Incident Pulse Width

The effect of incident laser pulse width is demonstrated in Figs. 4 and 5 for transmissivity and reflectivity, respectively. Four cases are selected for comparison, i.e., $t_p = 100$, 10, and 1 ps, and impulse. The impulse case (infinitesimal temporal pulse width) was broadly employed in previous studies.[19–26] The total laser energy per incident pulse is the same for all four cases. The number of ray emission bundles for the case of $t_p = 100$ ps is 10^8 in order to capture a fine time resolution. From Fig. 4, it is seen that the initial response time for the four cases remains the same. However, the transmissivity has a sudden increase for the cases when $t_p \leq 10$ ps. The first peak for the cases of impulse and $t_p = 1$ ps appears in a very short time, and its value is much larger than that for the case of $t_p = 10$ ps. After the first peak, the differences in transmissivity distribution among the three cases of $t_p = 1$, 10 ps, and impulse are minor. For the case of $t_p = 100$ ps ps, the direct transmission of photons is mixed with the scattering transmission so that no first narrow peak appears. The only peak appears around $t_p = 160$ ps and is purely the contribution of photons undergoing a large number of scattering events. The

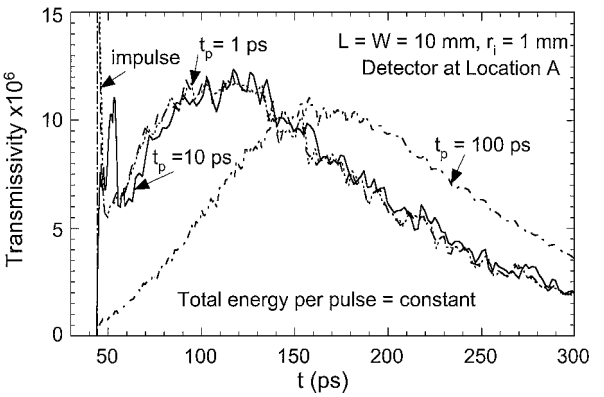

Fig. 4 Effect of incident laser pulse width on transient transmissivity distribution at location A.

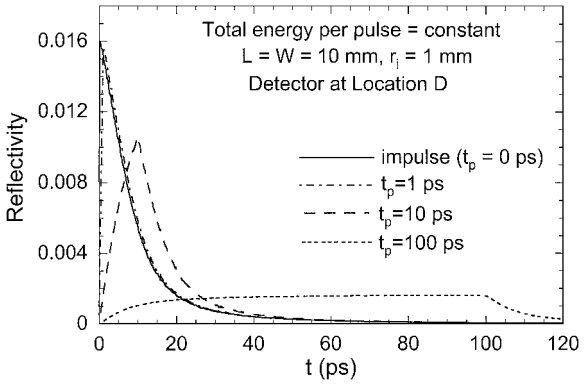

Fig. 5 Effect of incident laser pulse width on transient reflectivity distribution at location D.

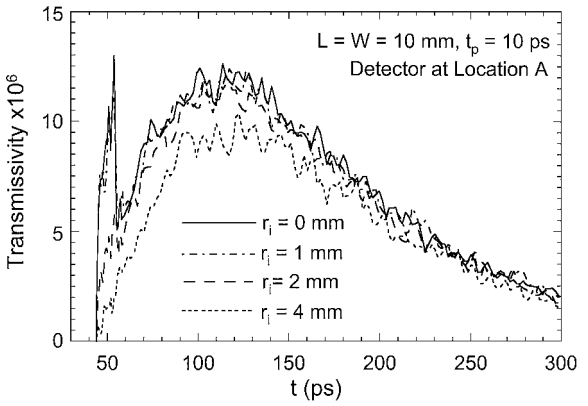

Fig. 6 Influence of laser beam radius on temporal transmissivity distribution at location A.

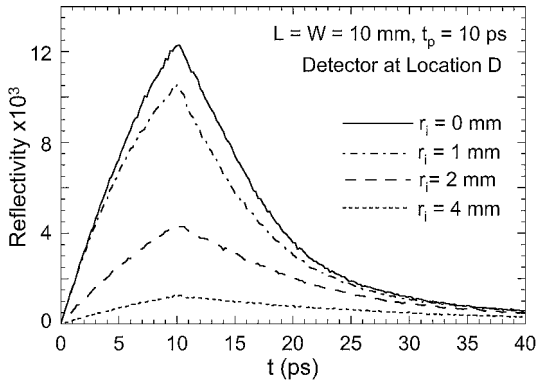

Fig. 7 Influence of laser beam radius on temporal reflectivity distribution at location D.

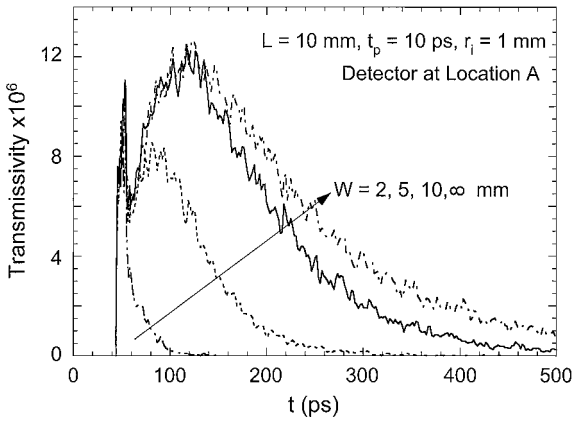

Fig. 8 Temporal transmissivity distributions for various lateral widths with $L = 10$ mm.

shape of the transmissivity distribution for $t_p = 100$ ps is obviously different from those of very short pulse width ($t_p \leq 10$ ps).

In Fig. 5, it is found that the influence of incident pulse width on reflectivity is more pronounced. The reflected pulse width increases as the incident pulse width increases. For the cases of $t_p = 10$ and 100 ps, the reflected pulse width is the same order as the incident pulse width. But the reflected pulse width is larger than the incident pulse width when $t_p \leq 1$ ps. The magnitude of reflectivity decreases as the incident pulse width increases. When $t_p \leq 10$ ps, the reflectivity increases suddenly until it reaches a maximum value around $t = t_p$ and then decreases rapidly for about 10 ps. After that, the reflectivity decreases gradually and has a long decaying tail. For a relatively long pulse width ($t_p = 100$ ps), there is a nearly flat reflectivity in the period from $t_p = 30$ to 100 ps. After that, the reflectivity decreases rapidly, forming a decaying tail.

From Figs. 4 and 5, it is found that the transmissivity and reflectivity distributions for impulse incident laser light are very similar to those for a very short pulse ($t_p = 1$ ps). If the incident pulse width is shorter than about a picosecond, it may be simulated by an impulse input. However, when $t_p \geq 10$ ps, an impulse simulation leads to incorrect transient transmissivity and reflectivity profiles.

Effect of Laser Beam Radius

Figure 6 shows the temporal transmissivity distributions at location A for an incident point source (infinitesimal beam radius) and Gaussian spatial profiles of $r_i = 1$, 2, and 4 mm, respectively. Other parameters have their basic values. The total energy per incident pulse remains constant for all cases. The first peak, which corresponds to direct light transport without scattering interaction, appears for the case of small incident beam radius ($r_i \leq 2$ mm). The smaller the beam radius, the stronger the first peak. After the first peak, it is hard to see the influence of incident laser beam radius on the transmissivity distributions when $r_i \leq 2$ mm. When $r_i = 4$ mm, the first peak disappears. This is because the incident flux is reduced, due to the increase in beam radius. Consequently, the transmissivity decreases when $r_i = 4$ mm. However, the incident beam radius has a slight effect on the decaying tail of the transmissivity. This occurs because the tail distribution is mainly attributed to the photons that have undergone a large number of scattering events and the tail distribution has little memory of the original photon incident positions.

The influence of incident beam radius on reflectivity at location D is further investigated in Fig. 7. It is observed that an increase in the incident beam radius reduces the magnitude of the reflectivity. However, the shapes of the temporal reflectivity profiles are similar for all of the incident beam radii. From Figs. 6 and 7, it is seen that the pulse width of the transmitted (except for the first peak) or reflected fluxes remains almost unchanged for various incident beam radii. Hence, the laser beam radius does not significantly influence the shape of the temporal transmissivity and reflectivity distributions. However, it obviously influences the magnitude of reflectivity.

Influence of the Medium's Dimensions

Figure 8 shows the temporal transmissivity profiles at location A for various lateral widths with constant thickness $L = 10$ mm. Other parameters have their basic values. It is a one-dimensional infinite slab problem when the width W is infinite. Because the lateral width does not influence the directly transmitted flux, the first peak does not obviously change for various lateral widths. However, the lateral width does strongly affect the shape and magnitude of the second transmitted pulse. With an increase of the lateral width, the strength of the transmissivity increases because less energy will be transmitted out of the medium from the lateral boundaries. For a larger width, the secondary peak occurs later and the transmitted pulse width enlarges. This is due to the effect of the radiation reflected from the lateral boundaries. For larger widths, the reflection path is greater and, therefore, the effect of reflected photons influences the transmissivity at much later time. For smaller widths, the

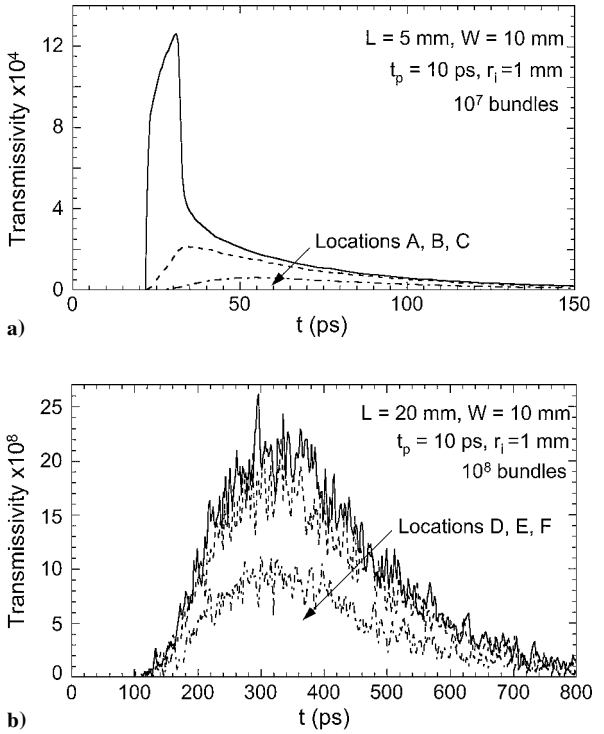

Fig. 9 Temporal transmissivity distributions at three different detector locations for a) $L = 5$ mm and b) $L = 20$ mm.

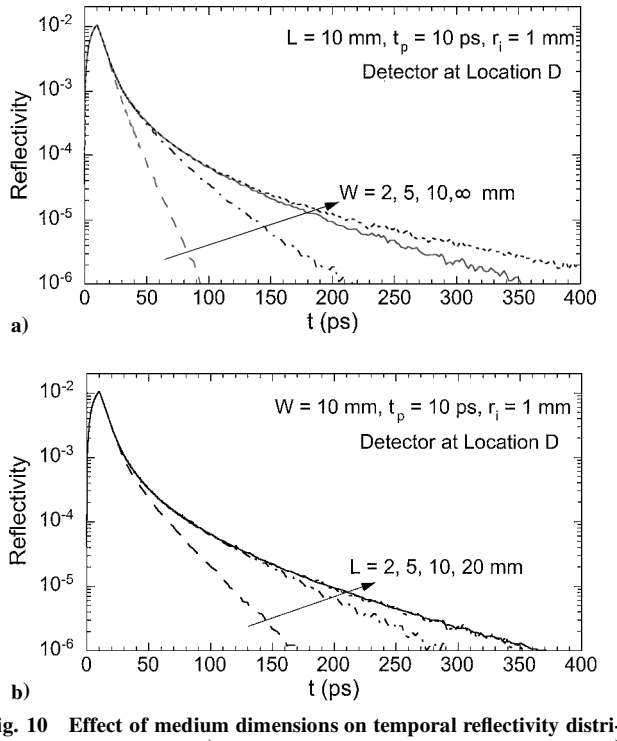

Fig. 10 Effect of medium dimensions on temporal reflectivity distribution at location D for a) various lateral widths with $L = 10$ mm and b) various medium thicknesses with $W = 10$ mm.

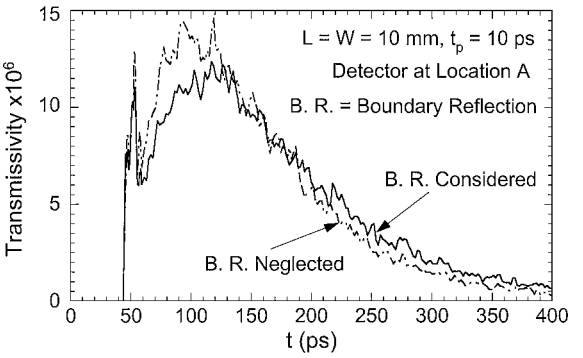

Fig. 11 Influence of boundary reflection on temporal transmissivity distribution at location A.

travel path is smaller for the reflected photons, and more radiation is transmitted through the medium from the lateral boundaries. As a result, no secondary peak appears for the case of very thin lateral width ($W = 2$ mm), and its decaying transmissivity tail is very short.

Figures 9a and 9b show the transmissivity distributions at three locations for a relatively optically thin medium ($L = 5$ mm) and an optically thick medium ($L = 20$ mm), respectively. Compared with the results of the step-input pulse in Fig. 2 ($L = 10$ mm), it is seen that the shape and magnitude of transmissivity are significantly influenced by the thickness of the medium. For a relatively optically thin medium ($L = 5$ mm), the first peak at location A is very strong because more radiation transmits directly without scattering, and the secondary peak at location A disappears. The magnitude of maximum transmissivity decreases considerably as the location moves from A to B to C. In contrast, for an optically thick medium ($L = 20$ mm), the first peak at location A due to direct transmission does not exist. The majority of transmitted flux comes from multiple scattering. The detector location influences only the magnitude of the transmissivity but does not influence the shape of the temporal transmissivity profile. From Fig. 2 and Figs. 9a and 9b, it is found that the transmitted flux pulse width enlarges as the thickness of the medium increases. However, the magnitude of transmissivity decreases substantially with increasing medium thickness.

The effect of the medium's dimensions on reflectivity distribution at location D is illustrated in Fig. 10a for various lateral widths and in Fig. 10b for various medium depths. It is seen that both the width W and thickness L of the medium have little effect on the maximum magnitude of reflectivity and on the temporal reflectivity distributions for times less than 20 ps. However, the dimensions do significantly affect the asymptotic log slope of reflectivity at longer time periods. The asymptotic log slope of reflectivity was used in the measurement[23–25] of optical properties of turbid media. For laterally thin media, after multiple scattering, photons tend to transmit through the lateral boundaries. Consequently, the reflectivity for long time periods reduces. This is why the logarithmic change of reflectivity versus time in the region $t > 20$ ps becomes steeper as the medium's lateral width decreases. When the medium's thickness is reduced, photons that have undergone a large number of scattering events tend to transmit through the medium rather than be backscattered. Hence, the reflectivity due to backscattering at long times is decreased when the medium thickness decreases. As a result, the logarithmic reflectivity decreases more quickly as the medium's thickness decreases. However, when the medium becomes optically very thick ($L \geq 10$ mm), any continued increase of medium thickness does not affect the reflectivity profile.

Effect of Boundary Reflection

The effect of boundary reflection due to the change of refractive index between different media is presented in Figs. 11 and 12. The boundary reflection referred to here is Fresnel reflection of the scattered radiation at interfaces of $z = 0$ and L. The effect of reflection of the incident laser light at the surface before it enters the medium has not been included. Parameters are selected using their basic values. The temporal transmissivity distributions at location A are depicted in Fig. 11 for the cases of boundary reflection considered and neglected. When boundary reflection is neglected, the maximum value of transmissivity is overestimated. This is because the radiation at the surface is assumed to be totally transmitted, and its reflected fraction is omitted. Moreover, the position of the secondary peak shifts to smaller time, and the transmitted pulse width is underestimated. These are identical to the findings of Takahashi et al.[25] in one-dimensional problems.

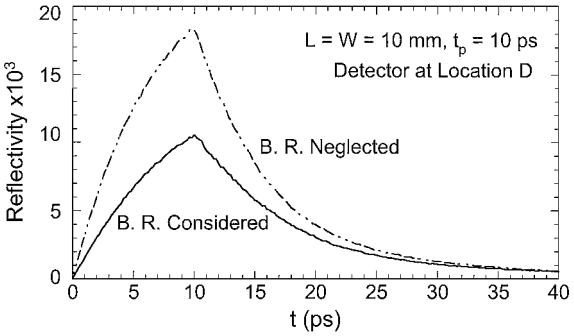

Fig. 12 Influence of boundary reflection on temporal reflectivity distribution at location D.

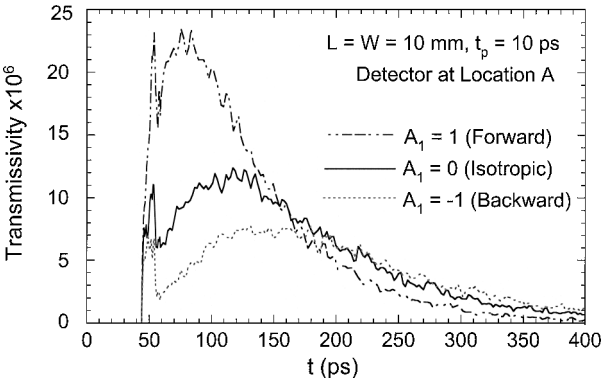

Fig. 13 Effect of anisotropic scattering characteristics on transmissivity distribution at location A.

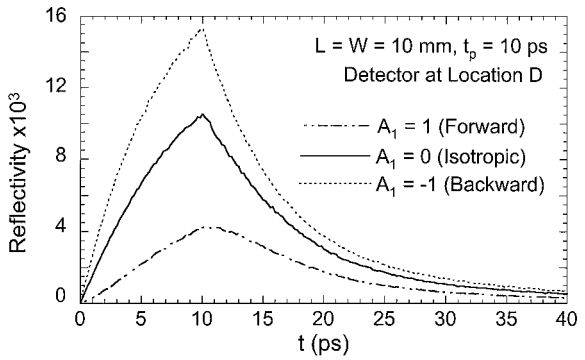

Fig. 14 Effect of anisotropic scattering characteristics on reflectivity distribution at location D.

The comparison of reflectivity at location D between the included and neglected boundary reflection is shown in Fig. 12. It is seen that neglecting the boundary reflection overestimates the maximum magnitude of the reflectivity. This is because a large number of photons, which hit the incident interface, will be reflected back into the medium due to Fresnel reflection. However, boundary reflection does not affect the time position of the maximum reflectivity and the reflected pulse width.

Effect of Anisotropic Scattering

Figures 13 and 14 disclose the influence of anisotropic scattering characteristics on the temporal transmissivity and reflectivity at locations A and D, respectively. A linear anisotropic scattering phase function is adopted. $A_1 = 1$ stands for strong forward scattering; $A_1 = 0$ stands for isotropic scattering; and $A_1 = -1$ stands for strong backward scattering. All parameters, except the phase function, have their basic values. It should be noted that the extinction coefficient and scattering albedo are the same for the three selected media, so the three media cannot be scaled into isotropically scattering media with the same equivalent scattering coefficient. Compared with the predictions from isotropic scattering, it is found from Fig. 13 that forward scattering shortens the transmitted pulse width, whereas backward scattering broadens the transmitted pulse width. This is because photons in a forward-scattering medium have the tendency to transmit through the medium quickly, but backward scattering increases the interaction events of light with the medium. This also leads to the time shift of the secondary peak in the transmissivity profiles. In Fig. 13, it is also seen that the magnitudes of the primary and secondary peaks are significantly affected by the anisotropic scattering characteristics. Forward scattering enhances the maximum value of the transmitted peaks, and backward scattering reduces the maximum value of the peaks. In contrast, it is seen from Fig. 14 that the maximum value of reflectivity is augmented by the backward-scattering medium but decreased by the forward-scattering medium. According to the isotropic scaling rule,[27] forward scattering can be scaled into isotropic scattering with a smaller scattering coefficient, and backward scattering can be modeled by isotropic scattering with an increased scattering coefficient. An augmented scattering coefficient will make it more difficult for the radiation to pass through the medium but easier for it to be reflected, and vice versa.

Numerical Uncertainty

The numerical uncertainty vs the number of emitted photon bundles is examined in Fig. 15. Convergent results are found for the three selected bundle numbers: 10^6, 10^7, and 10^8. With the increase of bundles, the magnitude of fluctuation becomes smaller and smaller. When 10^7 bundles are used in most of the present study, the relative statistical uncertainty for values of transmissivity is generally within 10%. However, we found that the prediction of reflectivity is much more accurate than that of transmissivity because the intensity of reflectivity is usually much larger than that of transmissivity in the present study. This is seen from Figs. 5, 7, and 14, where the reflectivity uncertainty is less than 3% compared to 10% for transmissivity.

In addition to the number of photons, the numerical uncertainty is also affected by other factors such as the optical thickness of the medium, the detector temporal resolution and detector area, and the intensity strength of the transmissivity and reflectivity. When the optical thickness increases, the numerical fluctuation is larger because fewer photons reach the detector. As shown in Fig. 9b, the fluctuation of the prediction is more profound for the case of $L = 20$ mm, even though 10^8 energy bundles were used in that case. However, the fluctuation is very small for the case of $L = 5$ mm, as shown in Fig. 9a, even though only 10^7 bundles were used. Increasing the detector temporal resolution and/or decreasing the detector area increase numerical uncertainty because fewer photons are collected by the detector.

For the first time, the present Monte Carlo algorithm has incorporated most of the known realistic physical conditions in processes of laser radiative interaction with scattering-absorbing media: anisotropic scattering, boundary reflection, medium dimensions, and temporal and spatial Gaussian distributions of the incident laser beam. An infinitesimal time-resolution technique was also developed. In steady-state radiative transfer, it is well known that the

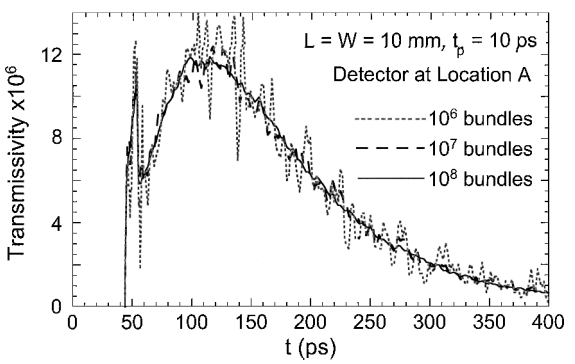

Fig. 15 Influence of photon bundle number on numerical uncertainty.

Monte Carlo model requires little storage. However, it should be noted that the storage used by the Monte Carlo method in transient radiative heat transfer increases substantially because the results are subject to time history. The computation cost is not a problem in the present scattering–absorbing medium because the medium's emission can be omitted for short-pulsed laser interaction and only the incident laser bundles are traced. With the presence of the emission of the medium, the computational time would increase because a large number of emission bundles from the medium should be traced. In addition, the CPU time increases as the scattering albedo increases. The present calculation for a forward anisotropically scattering medium with very high scattering albedo (0.997) takes about 80 min of CPU time (personal computer with Pentium III Xeon 500 MHz processor) when 10^7 energy bundles are employed.

Conclusions

The Monte Carlo method is formulated to simulate short-pulse laser radiation transport through multidimensional scattering-absorbing media. The temporal transmissivity and reflectivity distributions at different lateral locations are obtained by using various parameters, such as different boundary conditions, beam radii, incident pulse widths, medium widths and depths, and scattering anisotropies. The influences of these parameters are examined.

It is found that forward scattering enhances the transmitted pulse peak but reduces the pulse width; backward scattering decreases the transmitted pulse peak but augments the pulse width. Boundary reflection should be considered. Neglecting Fresnel reflection results in an overestimated maximum transmissivity and reflectivity and estimates a shorter transmitted pulse width. The assumption of impulse source is not good when the laser pulse width is much larger than 1 ps. When the incident pulse width is as large as 100 ps, the shape and spread of the transmissivity and reflectivity distributions are quite different from those of a very short incident pulse. The influence of incident beam radius on transmissivity is not significant for an optically thick medium. However, it strongly affects the magnitude of the reflectivity. The medium's dimensions significantly influence the temporal transmissivity and reflectivity distributions. As the lateral width decreases, the transmitted pulse width decreases and its secondary peak shifts to short time until it disappears for a very narrow lateral width. With an increase in medium thickness, the magnitude of the transmissivity decreases rapidly and the transmitted pulse width increases. The asymptotic logarithmic slope of reflectivity vs time is also significantly affected by the medium's dimensions. Thus, it is necessary to perform multidimensional simulation in short-pulsed laser transport processes.

Acknowledgments

The authors acknowledge partial support from the Sandia–National Science Foundation Joint Grant AW-9963 (CTS-973201) administered by Sandia National Laboratories, Shawn Burns, Project Manager.

References

[1]Kumar, S., and Mitra, K., "Microscale Aspects of Thermal Radiation Transport and Laser Applications," *Advances in Heat Transfer*, Vol. 33, 1998, pp. 187–294.

[2]Fork, R. L., Brito, J. Y., Cruz, C. H., Becker, P. C., and Shank, C. V., "Compression of Optical Pulses to Six Femtoseconds by Using Cubic Phase Compensation," *Optics Letters*, Vol. 12, 1987, pp. 483–485.

[3]Kumar, S., and Mitra, K., "Transient Radiative Transfer," *Proceedings of First International Symposium on Radiative Heat Transfer*, edited by M. P. Menguc, Begell House, New York, 1995, pp. 488–504.

[4]Kumar, S., Mitra, K., and Yamada, Y., "Hyperbolic Damped-Wave Models for Transient Light-Pulse Propagation in Scattering Media," *Applied Optics*, Vol. 35, No. 19, 1996, pp. 3372–3378.

[5]Mitra, K., Lai, M.-S., and Kumar, S., "Transient Radiation Transport in Participating Media Within a Rectangular Enclosure," *Journal of Thermophysics and Heat Transfer*, Vol. 11, No. 3, 1977, pp. 409–414.

[6]Mitra, K., and Kumar, S., "Development and Comparison of Models for Light-Pulse Transport Through Scattering-Absorbing Media," *Applied Optics*, Vol. 38, No. 1, 1999, pp. 188–196.

[7]Skocypec, R. D., and Buckius, R. O., "Photon Path Length Distributions for an Isotropically Scattering Planar Medium," *Journal of Quantitative Spectroscopy and Radiative Transfer*, Vol. 28, No. 5, 1982, pp. 425–439.

[8]Rackmil, C. I., and Buckius, R. O., "Numerical Solution Technique for the Transient Equation of Transfer," *Numerical Heat Transfer*, Vol. 6, 1983, pp. 135–153.

[9]Ishimaru, A., "Diffusion of a Pulse in Densely Distributed Scatters," *Journal of the Optical Society of America*, Vol. 68, 1978, pp. 1045–1050.

[10]Yamada, Y., "Light-Tissue Interaction and Optical Imaging in Biomedicine," *Annual Review of Heat Transfer*, Vol. 6, 1995, pp. 1–59.

[11]Yoo, K. M., Liu, F., and Alfano, R. R., "When Does the Diffusion Approximation Fail to Describe Photon Transport in Random Media," *Physical Review Letters*, Vol. 64, 1990, pp. 2647–2650.

[12]Siegel, R., and Howell, J. R., *Thermal Radiation Heat Transfer*, 3rd ed., Hemisphere, Washington, DC, 1992, Chap. 15.

[13]Modest, M. F., *Radiative Heat Transfer*, McGraw–Hill, New York, 1993, Chap. 19.

[14]Subramaniam, S., and Mengüc, M. P., "Solution of the Inverse Radiation Problem for Inhomogeneous and Anisotropically Scattering Media Using a Monte Carlo Technique," *International Journal of Heat and Mass Transfer*, Vol. 34, No. 2, 1991, pp. 253–266.

[15]Tong, T. W., and Skocypec, R. D., "Summary on Comparison of Radiative Heat Transfer Solutions for Specified Problems," *Developments in Radiative Heat Transfer*, ASME HTD-Vol. 203, American Society of Mechanical Engineers, New York, 1992, pp. 253–258.

[16]Farmer, J. T., and Howell, J. R., "Monte Carlo Prediction of Radiative Heat Transfer in Inhomogeneous, Anisotropic, Nongray Media," *Journal of Thermophysics and Heat Transfer*, Vol. 8, No. 1, 1994, pp. 133–139.

[17]Hsu, P.-F., and Farmer, J. T., "Benchmark Solutions of Radiative Heat Transfer Within Nonhomogeneous Participating Media Using the Monte Carlo and YIX Method," *Journal of Heat Transfer*, Vol. 119, No. 1, 1997, pp. 185–188.

[18]Yang, W. J., Taniguchi, H., and Kudo, K., "Radiative Heat Transfer by the Monte Carlo Method," *Advances in Heat Transfer*, Vol. 27, 1995, pp. 1–215.

[19]Wilson, B. C., and Adam, G., "A Monte Carlo Model for the Absorption and Flux Distributions of Light Tissue," *Medical Physics*, Vol. 10, 1983, pp. 824–830.

[20]Deply, D. T., Cope, M., van der Zee, P., Arridge, S., Wray, S., and Wyatt, J., "Estimation of Optical Path Length Through Tissue from Direct Time of Flight Measurement," *Physical Medicine Biology*, Vol. 33, No. 12, 1988, pp. 1433–1442.

[21]Jacques, S. L., "Time Resolved Propagation of Ultrashort Laser Pulses Within Turbid Tissues," *Applied Optics*, Vol. 28, No. 12, 1989, pp. 2223–2229.

[22]Flock, S. T., Patterson, M. S., Wilson, B. C., and Wyman, D. R., "Monte Carlo Modelling of Light Propagation in Highly Scattering Tissues—I: Model Predictions and Comparison with Diffusion Theory," *IEEE Transaction on Biomedical Engineering*, Vol. 36, No. 12, 1989, pp. 1162–1167.

[23]Madsen, S. J., Wilson, B. C., Patterson, M. S., Park, Y. D., Jacques, S. J., and Hefetz, Y., "Experimental Tests of a Simple Diffusion Model for the Estimation of Scattering and Absorption Coefficients of Turbid Media from Time-Resolved Diffusion Reflectance Measurements," *Applied Optics*, Vol. 31, No. 18, 1992, pp. 3509–3517.

[24]Hasegawa, Y., Yamada, Y., Tamura, M., and Nomura, Y., "Monte Carlo Simulation of Light Transmission Through Living Tissues," *Applied Optics*, Vol. 30, No. 31, 1991, pp. 4515–4520.

[25]Takahashi, Y., Yamada, Y., and Hasegawa, Y., "Effect of Fresnel Reflection on Time-Resolved Transmission Measurement," *Proceedings of SPIE, The International Society for Optical Engineering*, Vol. 2326, Bellingham, WA, 1994, pp. 495–504.

[26]Brewster, M. Q., and Yamada, Y., "Optical Properties of Thick, Turbid Media from Picosecond Time-Resolved Light Scattering Measurements," *International Journal of Heat and Mass Transfer*, Vol. 38, No. 14, 1995, pp. 2569–2581.

[27]Guo, Z., and Maruyama, S., "Scaling Anisotropic Scattering in Radiative Transfer in Three-Dimensional Nonhomogeneous Media," *International Communications in Heat and Mass Transfer*, Vol. 26, No. 7, 1999, pp. 997–1007.